IX. ELECTRODYNAMICS OF MEDIA

Academic and Research Staff

Prof. Hermann A. Haus
Prof. Jin Au Kong
Prof. Paul L. Penfield, Jr.
Prof. David H. Staelin
Dr. Leung Tsang

Graduate Students

Boucar Djermakoye
Howard L. Dyckman
Donald L. Lee
Eni G. Njoku

A. A NEW COUPLED-MODE APPROACH TO SPATIALLY PERIODIC SLAB MEDIA

JSEP

Joint Services Electronics Program (Contract DAAB07-75-C-1346)

Jin Au Kong

In the study of periodic media with applications to holography,[1] ultrasonic light diffraction,[2-4] and various active and passive components in integrated optics,[5-9] a coupled-mode approach proves to be the simplest method for getting results that can easily be interpreted physically. Conventional coupled-mode equations are first-order differential equations that can be derived directly from field equations by discarding terms involving second-order derivatives. Once these second-order terms are discarded, however, the boundary conditions for a given boundary problem can no longer be handled by these first-order equations. In this report we summarize the derivation and discuss the use of a new set of second-order coupled-mode equations. The solution to these equations is illustrated with reflection and transmission of a wave incident at the Bragg angle on a slab periodic medium.

Consider a periodic medium described by the permittivity

$$\epsilon(z) = \epsilon_2[1 + \eta \cos \kappa z] \tag{1}$$

where $\kappa = 2\pi/\Lambda$ and Λ is the periodicity. For the TE wave polarized in the $\hat{y}$ direction, the electric field E satisfies the wave equation

$$[\nabla^2 + \omega^2 \mu \epsilon(z)]\, E(x, z) = 0. \tag{2}$$

To facilitate the derivation of the coupled-mode equations, we let

$$E(x, z) = \sum_{m=-\infty}^{\infty} \phi_m(x)\, e^{im\pi/2}\, e^{i(k_z + m\kappa)z}, \tag{3}$$

where k_z is the $\hat{z}$-component of the wave vector. Substituting (3) in (2) and keeping only the two modal functions ϕ_0 and ϕ_{-1}, we arrive at

JSEP

JSEP

$$\frac{d^2\phi_o(x)}{dx^2} + \left[k_2^2 - k_z^2\right]\phi_o(x) - i\frac{\eta}{2}k_2^2\phi_{-1}(x) = 0 \tag{4}$$

$$\frac{d^2\phi_{-1}(x)}{dx^2} + \left[k_2^2 - (k_z-\kappa)^2\right]\phi_{-1}(x) + i\frac{\eta}{2}k_2^2\phi_o(x) = 0, \tag{5}$$

where $k_2 = \omega(\mu\epsilon_2)^{1/2}$.

Some comments should be made with regard to the coupled-mode equations (4) and (5). First, we obtain the conventional coupled-mode equations[1-5] by letting $\phi_m(x) = \psi_m(x)\exp(-ik_x x)$ in (4)-(5) and keeping the first-order derivative terms $d\psi_m/dx$. These equations have been studied extensively. It is interesting to compare the coupled-mode approach with the rigorous modal approach[5] where the modal functions are governed by Mathieu equations with the independent variable z instead of x, as shown in (4) and (5). Even though the rigorous modal approach gives rise to very accurate answers by keeping virtually all important modes, the results are numerical in nature. Coupled-mode equations (4) and (5) can be applied to cases wherein only two modes are of importance. The advantage is that we seek solutions that can be made to satisfy all given boundary conditions.

As an example, consider a plane wave incident at a periodic slab medium with boundaries at x = 0 and x = d (Fig. IX-1). The incident wave is at the Bragg angle, $\sin\theta = \kappa/2k_1$.

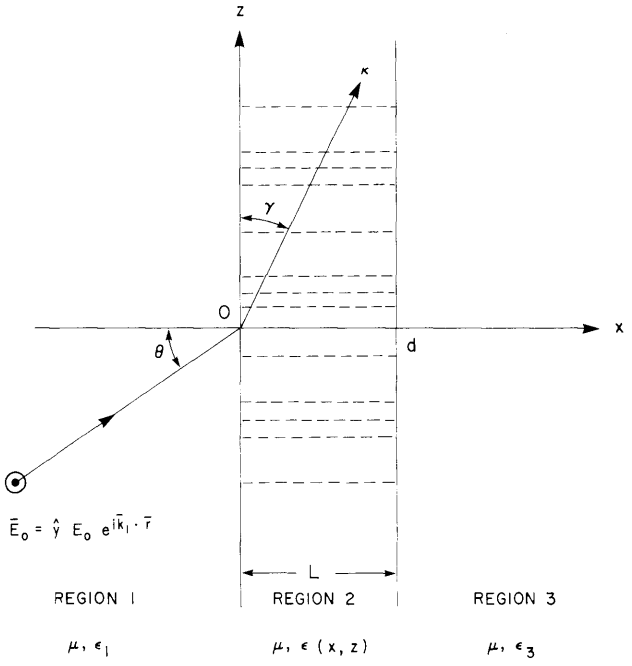

JSEP

Fig. IX-1. Geometrical configuration of the problem.

JSEP

There are 4 boundary conditions giving continuity of tangential electric and magnetic fields at x = 0 and x = d. There are 4 coupled modes inside the slab giving rise to 2 reflected modes with amplitudes R_o and R_{-1} and 2 transmitted modes with amplitudes T_o and T_{-1}. The z-component wave vector for all zero-order modes is $k_1 \sin\theta$, and for all -1-order modes $k_1 \sin\theta - \kappa$. Thus the 4 boundary conditions yield 8 linear simultaneous equations. The solutions for R_o, R_{-1}, T_o, and T_{-1} are

$$\begin{matrix} R_o \\ -1 \end{matrix} = \frac{1}{2}\left\{ \frac{\left(1 - \frac{k_{3x}}{k_{1x}}\right)\cos k_{2x}^- d - i\left(\frac{k_{3x}}{k_{2x}^-} - \frac{k_{2x}^-}{k_{1x}}\right)\sin k_{2x}^- d}{\left(1 + \frac{k_{3x}}{k_{1x}}\right)\cos k_{2x}^- d - i\left(\frac{k_{3x}}{k_{2x}^-} + \frac{k_{2x}^-}{k_{1x}}\right)\sin k_{2x}^- d} \right.$$

$$\left. \pm \frac{\left(1 - \frac{k_{3x}}{k_{1x}}\right)\cos k_{2x}^+ d - i\left(\frac{k_{3x}}{k_{2x}^+} - \frac{k_{2x}^+}{k_{1x}}\right)\sin k_{2x}^+ d}{\left(1 + \frac{k_{3x}}{k_{1x}}\right)\cos k_{2x}^+ d - i\left(\frac{k_{3x}}{k_{2x}^+} + \frac{k_{2x}^+}{k_{1x}}\right)\sin k_{2x}^+ d} \right\} \tag{6}$$

$$\begin{matrix} T_o \\ -1 \end{matrix} = \left\{ \frac{1}{\left(1 + \frac{k_{3x}}{k_{1x}}\right)\cos k_{2x}^- d - i\left(\frac{k_{3x}}{k_{2x}^-} + \frac{k_{2x}^-}{k_{1x}}\right)\sin k_{2x}^- d} \right.$$

$$\left. \pm \frac{1}{\left(1 + \frac{k_{3x}}{k_{1x}}\right)\cos k_{2x}^+ d - i\left(\frac{k_{3x}}{k_{2x}^+} + \frac{k_{2x}^+}{k_{1x}}\right)\sin k_{2x}^+ d} \right\} e^{-ik_{3x}d}, \tag{7}$$

where

$$k_{2x}^{\pm} = \sqrt{k_2^2 - \frac{\kappa^2}{4} \pm \frac{\eta}{2}k_2^2} \tag{8}$$

$$k_{1x} = \sqrt{k_1^2 - \frac{\kappa^2}{4}} \tag{9}$$

$$k_{3x} = \sqrt{k_3^2 - \frac{\kappa^2}{4}} \tag{10}$$

JSEP

JSEP

with $k_1 = \omega(\mu\epsilon_1)^{1/2}$ and $k_3 = \omega(\mu\epsilon_3)^{1/2}$. In (6) and (7) the upper sign is for the zero-order mode and the lower sign for the -1-order mode. When $\eta = 0$, the periodic medium becomes uniform and we see from (8) that $k_{2x}^{+} = k_{2x}^{-}$. Clearly, Eq. 6 gives $R_{-1} = 0$ and Eq. 7 gives $T_{-1} = 0$. There is no way to generate the -1-order modes. The solutions for R_o and T_o for this case reduce to the known values.[10]

References

1. H. Kogelnik, "Coupled Wave Theory for Thick Hologram Gratings," Bell Syst. Tech. J. 48, 2909-2947 (1969).
2. W. R. Klein and B. D. Cook, "Unified Approach to Ultrasonic Light Diffraction," IEEE Trans. on Sonics and Ultrasonics, Vol. SU-14, No. 3, pp. 123-134, July 1967.
3. P. Phariseau, "On the Diffraction of Light by Progressive Supersonic Waves," Proc. Indian Acad. Sci. 44, 165-170 (1956).
4. M. Born and E. Wolf, Principles of Optics (Pergamon Press, Oxford, 4th rev. ed., 1970).
5. R. S. Chu and J. A. Kong, "Modal Theory of Spatially Periodic Medium" (to appear in IEEE Trans. on Microwave Theory and Techniques).
6. R. E. Fontana, D. J. Epstein, and A. Linz, "Epitaxially Grown Single Crystal KTN for Thin Film Optical Modulators," 1975 IEEE/OSA Conference on Laser Engineering and Applications, Washington, D.C., May 28-30, 1975.
7. L. Kuhn, M. L. Dakss, P. F. Heidrich, and B. A. Scott, "Deflection of an Optical Guided Wave by a Surface Acoustic Wave," Appl. Phys. Letters 17, 265-267 (1970).
8. J. M. Hammer, D. J. Channin, M. T. Duffy, and C. C. Neil, "High-Speed Electrooptic Waveguide Grating Modulator Using Epitaxial ZnO," IEEE J. Quantum Electron., Vol. QE-11, No. 4, pp. 138-147, April 1975.
9. H. Kogelnik and C. V. Shank, "Simulated Emission in a Periodic Structure," Appl. Phys. Letters 18, 152-154 (1971).
10. J. A. Kong, Theory of Electromagnetic Waves (Wiley-Interscience, New York, 1975).

B. FIELDS OF A HORIZONTAL MAGNETIC DIPOLE ON THE SURFACE OF A TWO-LAYER UNIAXIAL MEDIUM

Joint Services Electronics Program (Contract DAAB07-75-C-1346)

David Y. D. Cheng, Jin Au Kong, Leung Tsang

Geophysical subsurface probing by the electromagnetic interference fringes (EIF) method has been investigated extensively,[1-5] with the use of a horizontal electric dipole antenna. Use of a horizontal magnetic dipole[6] reveals that such a source may be more effective in subsurface probing because its radiation pattern exhibits very sharp concentration of power in particular directions with the result that there are distinctive peaks in the interference plot. In this report we examine the radiation patterns and the

JSEP

interference plots with a horizontal magnetic dipole used to probe an anisotropic medium

with both uniaxial permittivity and permeability tensors.

Consider a horizontal magnetic dipole (HMD) placed on the surface of a uniaxially anisotropic medium characterized by

$$\bar{\bar{\epsilon}} = \epsilon_1 \begin{bmatrix} 1 & 0 & 0 \\ 0 & 1 & 0 \\ 0 & 0 & a \end{bmatrix}$$

$$\bar{\bar{\mu}} = \mu_1 \begin{bmatrix} 1 & 0 & 0 \\ 0 & 1 & 0 \\ 0 & 0 & b \end{bmatrix}$$

where the z axis is chosen to be perpendicular to the interface. In rectangular coordinates, the dipole is pointing in the x direction which corresponds to $\phi = 0$ either in the spherical or cylindrical coordinate systems. The reflection coefficient formulation and the saddle-point method are used to calculate the field components to first order in the asymptotic expansion. We define the ratio of the Poynting's radial vector component and the total power radiated by the HMD in free space to be the gain factor $G(\alpha_o, \phi)$, where $\alpha_o = \tan^{-1} \rho/z$ is the observation angle. From the field components, $G(\alpha_o, \phi)$ is calculated to be

$$G(\alpha_o, \phi) = \frac{3}{2}\left(\cos^2\alpha_o \left|T_{10}^{TE}\right|^2 \cos^2\phi + \left|T_{01}^{TM}\right|^2 \sin^2\phi\right) \tag{1}$$

in free space and

$$G_1(\alpha_o, \phi) = \frac{3}{2}\left(\frac{\epsilon_1}{\epsilon_o}\right)^{3/2}\left(\frac{\mu_1}{\mu_o}\right)^{1/2}\left[\frac{b^2 \cos^2\alpha_o \left|X_{01}\right|^2}{\left(b \sin^2\alpha_o + \cos^2\alpha_o\right)^{5/2}}\cos^2\phi + \frac{a^2\left|Y_{10}\right|^2}{\left(a \sin^{-2}\alpha_o + \cos^2\alpha_o\right)^{3/2}}\sin^2\phi\right] \tag{2}$$

in the anisotropic medium. In (1) and (2)

$$T_{10}^{TE} = \frac{2\mu_o\left(k_1^2 - k^2 \sin^{-2}\alpha_o/b\right)^{1/2}}{\mu_1 k \cos\alpha_o + \mu_o\left(k_1^2 - k^2 \sin^2\alpha_o/b\right)^{1/2}} \tag{3}$$

JSEP

$$T_{01}^{TM} = \frac{2\epsilon_1 k \cos \alpha_o}{\epsilon_1 k \cos \alpha_o + \epsilon_o\left(k_1^2 - k^2 \sin^{-2}\alpha_o/a\right)^{1/2}} \tag{4}$$

$$X_{01} = \frac{2\mu_1\left(k^2 - bk_1^2 \sin^{-2}\psi_o\right)^{1/2}}{\mu_o k_1 \cos \psi_o + \mu_1\left(k^2 - bk_1^2 \sin^{-2}\psi_o\right)^{1/2}} \tag{5}$$

$$Y_{10} = \frac{2\epsilon_o k_1 \cos \theta_o}{\epsilon_o k_1 \cos \theta_o + \epsilon_1\left(k^2 - ak_1^2 \sin^{-2}\theta_o\right)} \tag{6}$$

where

$$k_1 = \omega(\mu_1\epsilon_1)^{1/2}, \quad \theta_o = \tan^{-1}(a\rho/|z|), \quad \text{and} \quad \psi_o = \tan^{-1}(b\rho/|z|).$$

In Fig. IX-2a we plot the radiation pattern in the end-fire direction ($\phi = 0$) for different values of b. In Fig. IX-2b we plot the radiation pattern in the broadside direction ($\phi = 90°$)

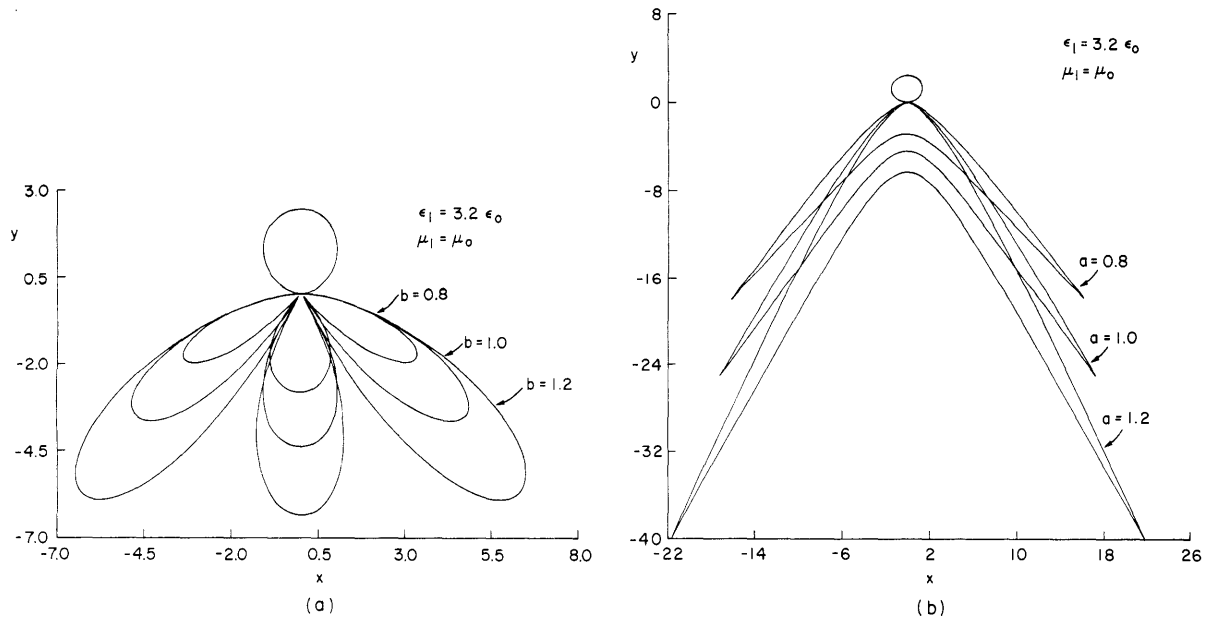

Fig. IX-2. Horizontal magnetic dipole half-space gain pattern. (a) End-fire ($\phi = 0°$). (b) Broadside ($\phi = 90°$).

for different values of a. Note the sharp peaks occurring at angles

JSEP

$$\alpha = \sin^{-1}(a^2n^2-(a-1))^{-1/2}. \tag{7}$$

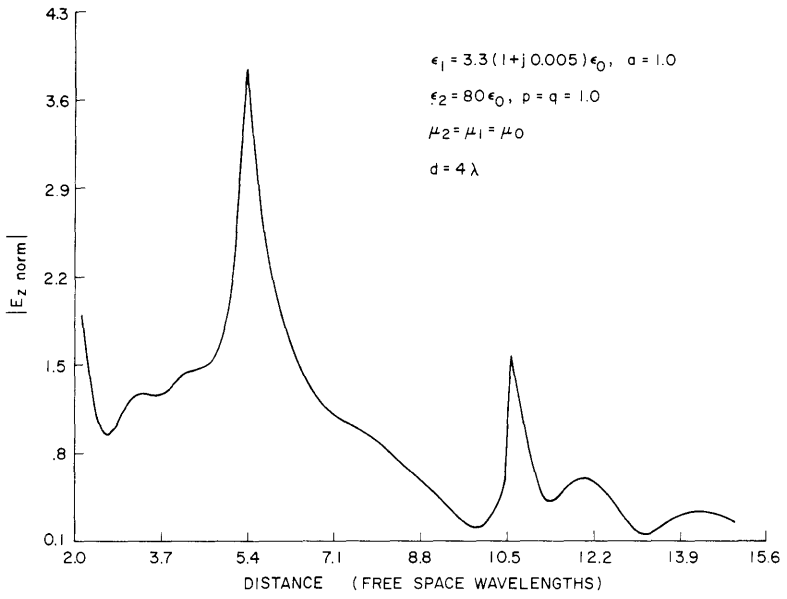

Fig. IX-3. Surface interference plot $|E_{z\ norm}|$. Broadside (two-layer case).

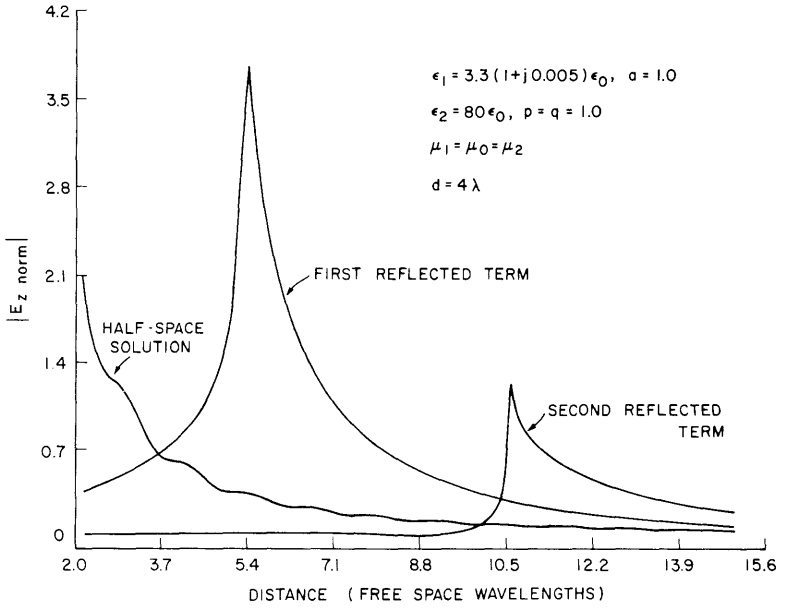

Fig. IX-4. Magnitude of various wave components in broadside surface $E_{z\ norm}$.

JSEP

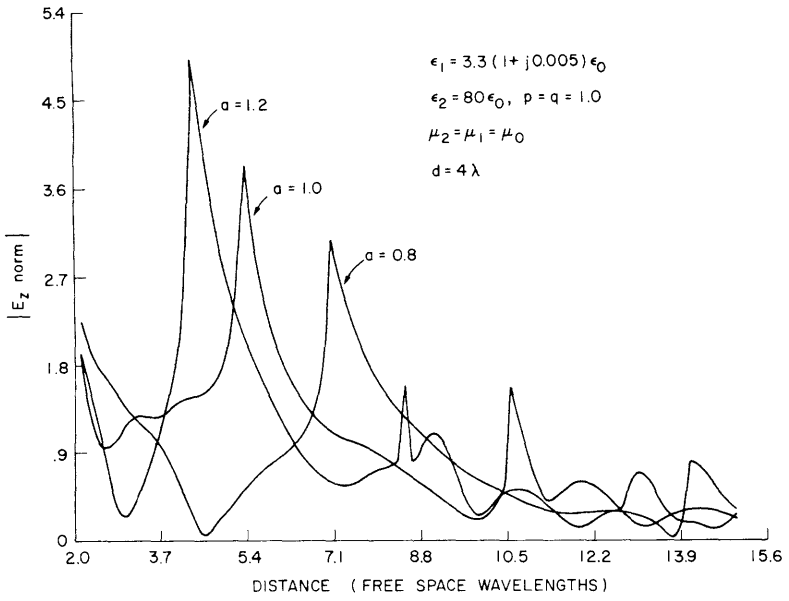

Fig. IX-5. Surface interference plot $|E_{z\ \text{norm}}|$. Broadside, 3 cases of uniaxiality.

This concentration of power launched into the medium will be displayed in sharp peaks in the interference patterns when there is a subsurface layer.

In the presence of a subsurface of another anisotropic medium we calculate the interference patterns as a function of distance from the dipole antenna. The subsurface is assumed to be at a distance d from the surface. To illustrate, in Fig. IX-3 we plot the magnitude of the z-component of the electric field $|E_z|$ in the broadside direction. Contributions that are due to the different wave components are shown in Fig. IX-4. To illustrate the effects of anisotropy, we plot $|E_z|$ for three different values of a in Fig. IX-5. We see that in the broadside direction the very sharp peak in the field plot is a very visible indication of a subsurface layer. These sharp peaks occur at distances $\rho = 2md/a(n^2a-1)$. Comparing these results with those calculated with the use of a horizontal electric dipole,[5] we conclude that a horizontal magnetic dipole provides a clearer indication of the depth of a subsurface for both isotropic and anisotropic media.

References

1. J. A. Kong, "Electromagnetic Fields Due to Dipole Antennas over Stratified Anisotropic Media," Geophysics 37, 985-996 (1972).

2. L. Tsang, J. A. Kong, and G. Simmons, "Interference Patterns of a Horizontal Electric Dipole over Layered Dielectric Media," J. Geophys. Res. 78, 3287-3300 (1973).

3. J. A. Kong, L. Tsang, and G. Simmons, "Geophysical Subsurface Probing with Radio-Frequency Interferometry," IEEE Trans. on Antennas and Propagation, Vol. AP-22, No. 4, pp. 616-620, July 1974.

JSEP

4. L. Tsang and J. A. Kong, "Electromagnetic Fields Due to a Horizontal Electric Dipole Antenna Laid on the Surface of a Two-Layer Medium," IEEE Trans. on Antennas and Propagation, Vol. AP-22, No. 5, pp. 709-711, September 1974.

5. L. Tsang and J. A. Kong, "Application of the Radio-Frequency Interferometry Method to a Stratified Anisotropic Medium," IEEE Trans. on Antennas and Propagation, Vol. AP-23, No. 5, pp. 725-728, September 1975.

6. J. A. Kong, W. C. Chan, and L. Tsang, "Geophysical Subsurface Probing with the Electromagnetic Interference Fringes (EIF) Method," in Program and Abstracts of USNC/URSI 1975 Annual Meeting, University of Colorado, Boulder, Colorado, October 20-23, 1975, Session VI-10, p. 258.

JSEP

C. MICROWAVE REMOTE SENSING OF TWO-LAYER MEDIA WITH DISCRETE SCATTERERS AND RANDOM FLUCTUATIONS

Joint Services Electronics Program (Contract DAAB07-75-C-1346)

Leung Tsang, Jin Au Kong

In low-conductivity areas, such as snow, ice-covered land or water, desert and lunar areas, subsurface layering and scattering are dominant factors affecting brightness temperatures observed in microwave passive remote sensing. By using the model of a half space, various theories have been developed in the study of subsurface scattering effects on brightness temperatures.[1-4] By employing the Rayleigh phase function, England[5] examined emission darkening caused by a two-layer scattering medium. His results are only applicable to the low-frequency regime. For a two-layer random medium with laminar structure, a wave approach employing the Dyson and the Bethe-Salpeter equations has been used to devise a modified radiative transfer approach.[6,7]

In this report, we use the radiative transfer approach to study thermal microwave emission from a two-layer medium composed of a slab of scatterers overlying a homogeneous half space. Two scattering models are used, one that has three-dimensional random fluctuations of permittivity and another with discrete spherical scatterers. Mie scattering phase functions are employed in the second model.

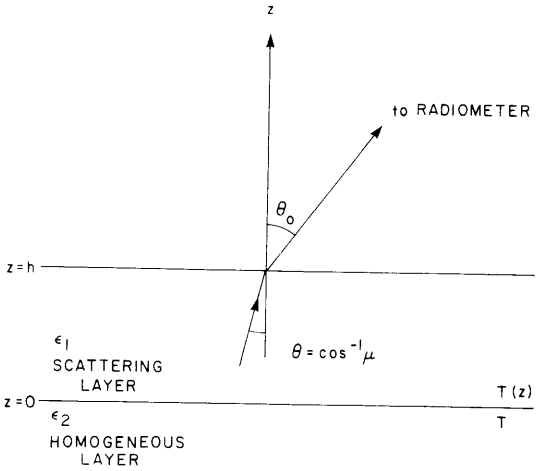

Fig. IX-6.
Geometry of the problem.

Consider a scattering dielectric slab of thickness h and permittivity $\epsilon_1 = \epsilon_1' + i\epsilon_1''$ (medium 1) overlying a homogeneous half space of permittivity $\epsilon_2 = \epsilon_2' + i\epsilon_2''$ (medium 2) as shown in Fig. IX-6. Both medium 1 and medium 2 are emitting thermal

JSEP

JSEP radiation. Medium 1 has temperature distribution T(z) and medium 2 has constant temperature T. The radiative transfer equations inside medium 1 have the form

$$\mu \frac{dI_\beta}{dz}(z,\mu,h) = \kappa_a(T(z)) - \kappa_{e\beta}(\mu)\, I_\beta(z,\mu,h) + \sum_{\alpha=v,h} \int_{-1}^{1} d\mu'\, (\beta(\mu), \alpha'(\mu'))\, I_{\alpha'}(z,\mu',h), \qquad (1)$$

where $\beta = v, h$, and $-1 < \mu < 1$.

In (1) $I_v(z,\mu,h)$ and $I_h(z,\mu,h)$ denote the specific intensities for the vertical and horizontal polarizations at angle $\theta = \cos^{-1}\mu$, κ_a and $\kappa_{e\beta}(\mu)$ are the absorption and extinction coefficients for polarization β, and $(\beta(\mu), \alpha'(\mu'))$ are the scattering phase functions. The absorption and extinction coefficients and the scattering phase functions for three-dimensional random media and for spherical scatterers are given elsewhere.[8] The boundary conditions for the radiative transfer equations for $0 < \mu < 1$, at $z = h$ are

$$I_\beta(h,-\mu,h) = r_{01\beta}(\mu)\, I_\beta(h,\mu,h) \qquad (2a)$$

and, at $z = 0$

$$I_\beta(0,\mu,h) = r_{12\beta}(\mu)\, I_\beta(0,-\mu,h) + t_{12\beta}(\mu)\, CT, \qquad (2b)$$

where $r_{01\beta}(\mu)$ and $t_{01\beta}(\mu)$ are the Fresnel reflectivity and trnasmissivity at angle θ for polarization β at the boundary $z = h$, and $r_{12\beta}(\mu)$ and $t_{12\beta}(\mu)$ are the Fresnel reflectivity and transmissivity at $z = 0$. The boundaries are assumed to be quasi-specular so that wave interference phenomena are effectively averaged.[5] In Eq. 3, $C = \epsilon_1' \kappa/\epsilon_o \lambda^2$, where κ is Boltzmann's constant and λ is the free space wavelength. The brightness temperature T_B as observed by a radiometer at angle θ_o is

$$T_{B_\beta}(\theta_o, h) = \frac{1}{C} t_{01\beta}(\mu)\, I_\beta(h,\mu,h) \qquad (3)$$

with θ_o and $\theta = \cos^{-1}\mu$ related by Snell's law. The radiative transfer equations are solved by casting them in quadrature form with the use of the Legendre polynomial $P_{2n}(\mu)$.

For the random-medium model the mean permittivity is ϵ_1, and the covariance function of the random part of permittivity, $\epsilon_f(\bar{r})$, is taken to be

$$\langle \epsilon_f(\bar{r}_1)\, \epsilon_f^*(\bar{r}_2) \rangle = \frac{\delta k_1'^4}{\omega^4 \mu_o^2} \exp\left(-\frac{|z_1 - z_2|}{\ell}\right) \exp\left(-\frac{|x_1 - x_2|^2 + |y_1 - y_2|^2}{\ell_\rho^2}\right), \qquad (4)$$

where k_1' is the real part of the mean wave number, ω is the angular frequency, μ_o is the free space permeability, δ is the variance of the fluctuations, and ℓ and ℓ_ρ are the

JSEP correlation lengths in vertical and horizontal directions. For the case of discrete

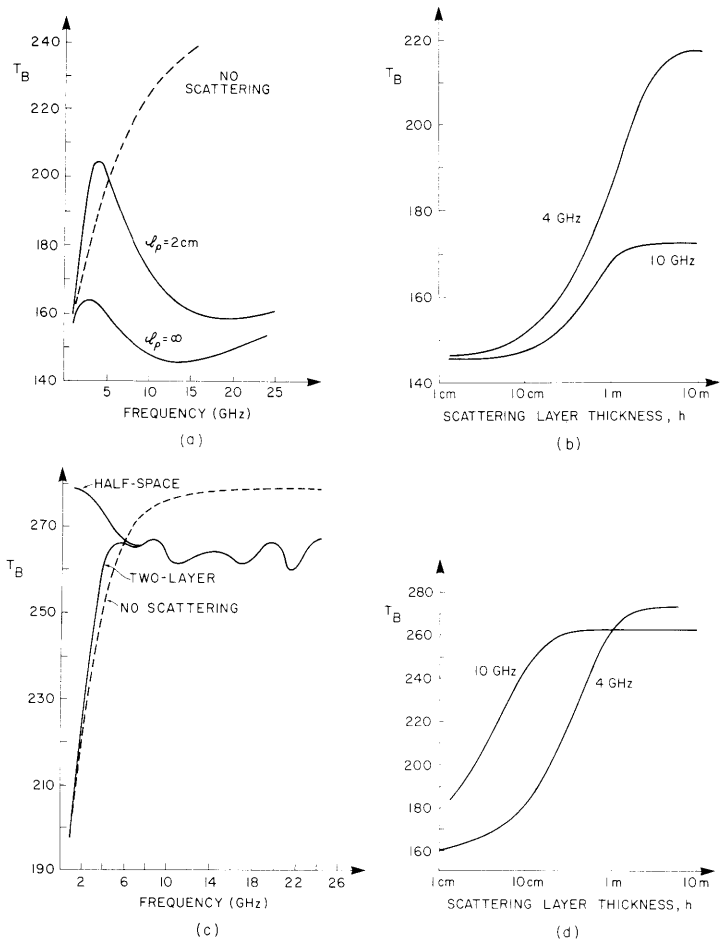

Fig. IX-7. (a) Brightness temperature vs frequency with $\epsilon_1 = 3.2(1+i0.0009)\epsilon_o$, $\epsilon_2 = 77.2(1+i0.17)\epsilon_o$, h = 2 m, T = 273 K for both media, ℓ = 1 mm, δ = 0.02, and two ℓ_ρ. For broken-line curve δ = 0.

(b) Brightness temperature vs scattering layer thickness with $\epsilon_1 = 3.2(1+i0.0009)\epsilon_o$, $\epsilon_2 = 77.2(1+i0.17)\epsilon_o$, T = 273 K for both media, ℓ_ρ = 2 cm, ℓ = 1 mm, δ = 0.02, and two frequencies.

(c) Brightness temperature vs frequency with $\epsilon_1 = 3(1+i0.0053)\epsilon_o$, $\epsilon_s = 8.3\epsilon_o$, a = 5 mm, f = 0.03, $\epsilon_2 = 77.2(1+i0.17)\epsilon_o$, T = 300 K for both media, and h = 1 m. The half-space case is shown for comparison. For broken-line curve f = 0.

(d) Brightness temperature vs scattering layer thickness with $\epsilon_1 = 3(1+i0.0053)\epsilon_o$, $\epsilon_s = 8.3\epsilon_o$, a = 5 mm, f = 0.03, $\epsilon_2 = 77.2(1+i0.17)\epsilon_o$, T = 300 K for both media, and two frequencies.

JSEP

scatterers, they are taken to be spherical and are characterized by permittivity ϵ_s and radius a. The fractional volume occupied by the spherical scatterers is f. Mie scattering phase functions are used in the radiative transfer equations.

In Fig. IX-7a we plot the brightness temperatures as a function of frequency for random media of two different lateral correlation lengths. The minimum of brightness temperature is a result of resonant scattering and cannot be uncovered if a Rayleigh phase function is used.[5] In the presence of finite lateral variations the location of the minimum is also shifted with respect to that of no lateral variations ($\ell_\rho \to \infty$). The presence of the subsurface reflector introduces a maximum in the low-frequency side. Also shown in Fig. IX-7a and IX-7c (broken lines) is the case when scattering is absent. We note that scattering can both increase and decrease the brightness temperature. In Fig. IX-7b we plot the brightness temperature as a function of layer thickness at two frequencies. We note that the brightness temperatures increase monotonically before approaching a constant value at large layer thicknesses. The curves in Fig. IX-7b have been calculated by using the invariant imbedding technique.[3] The parameters in Fig. IX-7a and IX-7b are for the case of a layer of ice over water.

In Fig. IX-7c we plot the brightness temperature as a function of frequency. We note that the brightness temperature first rises when frequency increases before exhibiting multiple resonant behavior that is characteristic of Mie scattering. In Fig. IX-7d we have also used the invariant imbedding technique to calculate the brightness temperature as a function of layer thicknesses at two different frequencies. We note that there is a point of intersection for the two curves at approximately 1-m thickness. The reason for this is that the effect of the subsurface reflector is dominant at small layer thicknesses, while the scattering properties of the slab are more important at large layer thicknesses.

References

1. A. S. Gurvich, V. I. Kalinin, and D. T. Matveyev, "Influence of the Internal Structure of Glaciers on Their Thermal Radio Emission," Atmospheric and Oceanic Phys. 9, 712-717 (1973).
2. A. W. England, "Thermal Microwave Emission from a Half-space Containing Scatterers," Radio Sci. 9, 447-454 (1974).
3. A. Stogryn, "Electromagnetic Scattering by Random Dielectric Constant Fluctuations in a Bounded Medium," Radio Sci. 5, 509-518 (1974).
4. L. Tsang and J. A. Kong, "The Brightness Temperature of a Half-space Random Medium with Nonuniform Temperature Profile," Radio Sci. 10, 1025-1033 (1975).
5. A. W. England, "Thermal Microwave Emission from a Scattering Layer," J. Geophys. Res. 80, 4484-4496 (1975).
6. L. Tsang and J. A. Kong, "Microwave Remote Sensing of a Two-Layer Random Medium," IEEE Trans. on Antennas and Propagation, Vol. AP-24, No. 3, pp. 283-288, May 1976.
7. L. Tsang and J. A. Kong, "Microwave Remote Sensing of a Two-Layer Random Medium. II," Electrodynamics Memo. No. 48, M. I. T., March 1, 1976.
8. L. Tsang and J. A. Kong, "Thermal Microwave Emission from Half-space Random Media" (to appear in Radio Sci.).

JSEP